UNIVERSITÀ DEGLI STUDI DI BERGAMO
DIPARTIMENTO DI INGEGNERIA DELL'INFORMAZIONE
E METODI MATEMATICI°

QUADERNI DEL DIPARTIMENTO

Department of Information Technology and Mathematical Methods

Working Paper

Series "*Mathematics and Statistics*"

n. 2/MS – 2011

Applications of Variational Data Assimilation in Computational Hemodynamics

by

M. D'Elia, L. Mirabella, T. Passerini, M. Perego, M. Piccinelli, C. Vergara, A. Veneziani

° Viale Marconi. 5, I – 24044 Dalmine (BG), ITALY, Tel. +39-035-2052339; Fax. +39-035-562779

[§] L'accesso alle *Series* è approvato dal Comitato di Redazione. I *Working Papers* della Collana dei Quaderni del Dipartimento di Ingegneria dell'Informazione e Metodi Matematici costituiscono un servizio atto a fornire la tempestiva divulgazione dei risultati dell'attività di ricerca, siano essi in forma provvisoria o definitiva.

Applications of Variational Data Assimilation in Computational Hemodynamics

Marta D'Elia, Lucia Mirabella, Tiziano Passerini, Mauro Perego, Marina Piccinelli, Christian Vergara and Alessandro Veneziani

Abstract The development of new technologies for acquiring measures and images in order to investigate cardiovascular diseases raises new challenges in scientific computing. These data can be in fact merged with the numerical simulations for improving the accuracy and reliability of the computational tools. Assimilation of measured data and numerical models is well established in meteorology, whilst it is relatively new in computational hemodynamics. Different approaches are possible for the mathematical setting of this problem. Among them, we follow here a variational formulation, based on the minimization of the mismatch between data and numerical results by acting on a suitable set of control variables. Several modeling and methodological problems related to this strategy are open, such as the analysis of the impact of the noise affecting the data, and the design of effective numerical solvers. In this chapter we present three examples where a mathematically sound (variational) assimilation of data can significantly improve the reliability of the numerical models. *Accuracy* and *reliability* of computational models are increasingly important features in view of the progressive adoption of numerical tools in the design of new therapies and, more in general, in the decision making process of medical doctors.

M. D'Elia, T. Passerini, M. Piccinelli, A. Veneziani
Department of Mathematics and Computer Science, Emory University, 400 Dowman Dr, 30322, Atlanta GA (USA), e-mail: {marta,tiziano,marina,ale}@mathcs.emory.edu

L. Mirabella
W.H. Coulter Department of Biomedical Engineering, Georgia Institute of Technology, 315 Ferst Dr., 30332 Atlanta GA (USA) e-mail: lucia.mirabella@bme.gatech.edu

M. Perego
Department of Scientific Computing, Florida State University, Tallahassee FL (USA) e-mail: mperego@fsu.edu

C. Vergara
Department of Information Engineering and Mathematical Methods, University of Bergamo, Italy e-mail: christian.vergara@unibg.it

1 Introduction

In the last 20 years mathematical and numerical models have been progressively used as a tool for supporting medical research in the cardiovascular science. *In silico* experiments can provide remarkable insights into a physio-pathological process completing more traditional *in vitro* and *in vivo* investigations. Numerical models have been playing the role of "individual based" simulators, able to furnish a dynamical representation of the biology of a specific patient as a support to the prognostic activity. At the same time, the need for quantitative responses for diagnostic purposes has strongly stimulated the design of new methods and instruments for measurements and imaging. On the one hand, we can simulate in 3D large portions of the cardiovascular system of a real patient properly including simplified models for the peripheral sites (see e.g. [73, 72, 33, 23, 65]). On the other hand, thanks to new instruments, images and measures nowadays provide doctors and bioengineers with a huge amount of data. These data offer obviously new possible benchmarks for the numerical simulations (see e.g. [37]). However, beyond the validation, it is possible to merge simulations and measures by means of more sophisticated numerical techniques. This procedure is called *Data Assimilation* (DA) (see e.g. [7]). With this name we mean the ensemble of methods for merging observed (generally sparse and noisy) information into a numerical model based on the approximation of physical and constitutive laws. The merging improves the quality of the information brought both by numerical results and by measurements:
- numerical simulations are improved by the merging of data that allow to include effects otherwise difficult to model (at the qualitative or quantitative level), such as the presence of tissues surrounding an artery or the motion of heart affecting the aortic dynamics;
- measures are in general affected by noise, so that assimilation of results based on physical and constitutive laws introduces a sophisticated filter, forcing the consistency with basic principles.

In some fields, these techniques are quite mature and tested, in particular in geophysics and meteorology (see the excellent review of methods in [7]). There are basically two classes of methods for performing DA, both with pros and cons.

Variational Methods DA is performed by minimizing a functional, estimating the discrepancy between numerical results and measures. The optimization problem is solved by using the mathematical model as a constraint, upon the identification of a proper set of control variables. In environmental studies this is often the initial state of the system of interest. In some cases (*Nudging* or *Dynamic Relaxation Methods*) the functional to be minimized is properly "altered" so to include the data to be assimilated directly in the equations of the model.

Stochastic methods These are based on the extension to nonlinear problems of the *Kalman filter*, which is a statistical approach for prediction of linear systems affected by uncertainty [69, 41, 81], relying upon a Bayesian maximum likelihood argument.

On the contrary, there are relatively few studies devoted to a mathematically sound assimilation of data in hemodynamics, probably because the availability of more and more accurate measurements is the result of truly recent advancements. In particular, we mention [11, 51, 52, 53, 70], essentially based on Kalman filtering techniques, and [26] for the variational approach.

In this chapter we consider three possible applications of DA based on *variational methods*. In particular we present possible techniques for

1. merging velocity data into the numerical solution of the incompressible Navier-Stokes equations, so to eventually retrieve non primitive variables like the *Wall Shear Stress* (WSS);
2. including images into the simulation of blood flow in a moving domain, so to perform the fluid dynamics simulations including the measured movement of the vessel;
3. estimating physiological parameters of clinical interest by matching numerical simulations and available data.

In all these examples we face a common structure that can be depicted as a classical feedback loop illustrated in the scheme below.

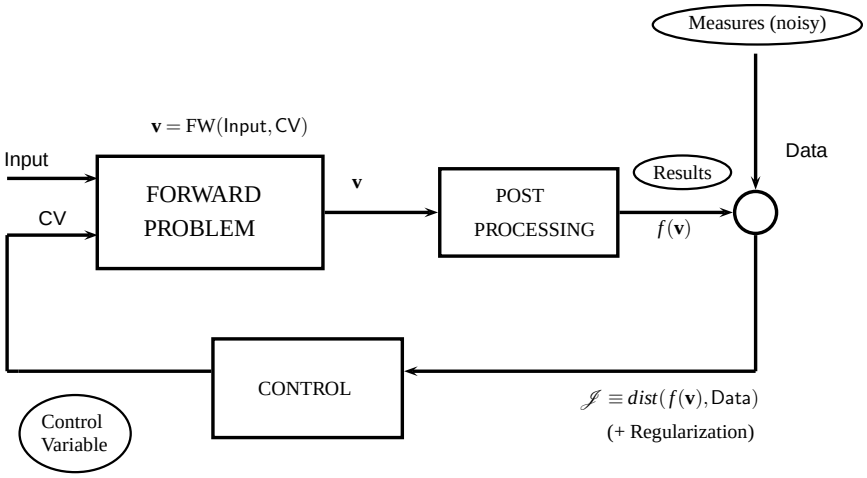

At an abstract level, all these applications actually lead to solve a problem in the form: Find the Control Variable CV (belonging to a suitable functional space) such that it minimizes the distance

$$\mathscr{J} \equiv dist(f(\mathbf{v}, \mathsf{Data})) \quad (+ \text{ Regularization}), \tag{1}$$

where Data is the set of (noisy) measures, $\mathbf{v}$ the solution of the Forward Problem FW, which depends on some Input variables and CV. Finally, $f(\cdot)$ represents a post processing step for computing the quantity to be compared with the data. "Regularization" stands for some possible Tikhonov-like regularizing term with the role of making the mathematical and numerical problem more tractable (see e.g. [19, 34]). Control problems with constraints represented by partial differential equations have

been studied since a long time ([44, 46, 47, 30, 31, 45, 87, 34]). In computational hemodynamics, these problems have been considered, for example, for the prescription of defective boundary conditions [21, 24, 25].

There are several issues when solving these kind of problems. Particularly relevant for our applications are

1. The *existence* of an admissible CV that attains the minimal distance between data and results. This can depend on the location (in space and time) of the available data and can be forced by a proper regularization term;
2. The *noise* that invariably affects the data to be assimilated; this has a major impact on the reliability of the entire data assimilation process.

In the examples presented below we will partially address these issues, pointing out available results and open problems for each application. We will split each example in three sections after the presentation of the specific problem and its medical motivations, namely (i) the formalization of the problem in mathematical and numerical terms - with a specific link to the feedback loop above - (ii) the discussion of some preliminary numerical results and (iii) of the associated prospective research. Far from being a conclusive review of methods and applications, the present work pinpoints several open challenging problems in the adoption of variational methods for DA in computational hemodynamics. These are anticipated to become an important tool for pursuing more reliability of numerical simulations in the general perspective of *data driven simulations* [12] and *inverse cardiovascular mathematics*. Accuracy and reliability of scientific computing are in fact an increasingly critical issue for the progressive inclusion of numerical simulations in the validation protocol of medical devices/drugs as well as in the decision making of medical doctors [20].

2 Variational Assimilation of Velocity Data for the Incompressible Navier-Stokes Equations

Bicuspid aortic valve (BAV) is the most common congenital heart defect, occurring in about 1% of the population [38]. At a mean age of 17.8 years 52% of males with normally functioning BAV already have aortic dilatation [80] which may eventually lead to aortic regurgitation or dissection or aortic aneurysms. Medical doctors are interested in developing a better understanding of the hemodynamics contributing to aortic dilatation not only in patients with BAV but also in other forms of congenital heart disease in which aortic dilatation is common [68]. Such an understanding may allow early risk stratification, possibly leading to guidelines for earlier intervention in high-risk groups, with an anticipated resultant reduction in morbidity and mortality for these patients. Some studies suggest that BAV morphology results in abnormal flow patterns in the ascending aorta, anticipating that valves with significant asymmetry would result in highly disturbed flow patterns. Consequently, the flow patterns, as detected by MRI flow-velocity encoding methodologies (see Fig.

1), have predictive value in determining which BAV morphology variants would be at greater risk of developing aortic dilatation. In order to validate this hypothesis,

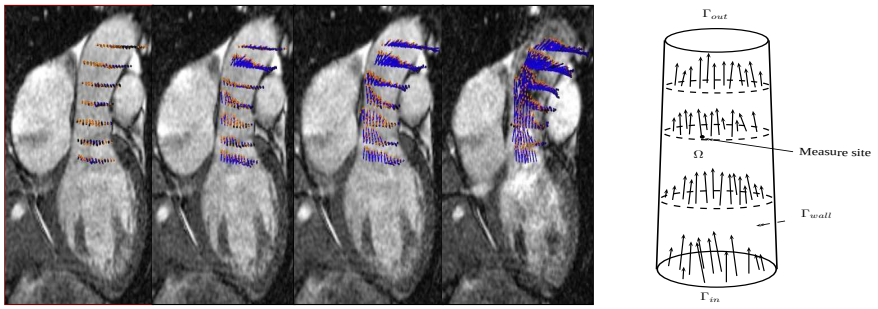

Fig. 1 Left: Blood velocity measured with Magnetic Resonance in the ascending aorta of a patient, reproduced with permission from [15]. Right: example of a possible region of interest Ω with velocity measures inside the domain.

clinical studies have been performed [35, 15] evaluating the WSS in BAV patients from MRI measurements. WSS is computed by a finite difference approximation based upon the velocity data and the blood viscosity measure. However, these estimates are clearly affected by both the discretization error and the noise of the data. Numerical simulations of blood flow can be carried out in the region of interest to improve this computation (see e.g. [78]). In this context, measures inside the domain of interest are not strictly needed for solving the incompressible fluid problem, that requires only initial and boundary conditions. However, they can be merged with the numerical results for obtaining a better estimate of the WSS. This leads to the following problem: How is it possible to incorporate velocity (noisy) data available in a domain of interest into the computation of the incompressible Navier-Stokes equations? A similar problem in the context of the fluid mechanics of the heart has been studied in [37] (and successively analyzed in [17]). In this work, available velocity data belong to a plane cutting the domain. As it has been observed in [37, 14], in principle, if the data belong to surfaces that split the region of interest into regular subdomains (as a plane), an immediate approach for the assimilation would be to solve the equations in each subdomain. In fact, the available data can be prescribed as standard boundary conditions. This naif approach, however, does not consider the presence of the noise. As a matter of fact, no filtering is introduced in this way and the noise is spread into each subdomain, resulting in significant inaccuracies (see [14]). For this reason, we resort here to a variational approach.

2.1 Mathematical formulation and numerical approximation

Let us denote by Ω a domain in $\mathbb{R}^d$ ($d = 2, 3$; in real applications $d = 3$, however here we limit numerical results to the 2D case). We assume that the domain of interest Ω (see Fig. 1, right) features an inflow boundary Γ_{in}, an outflow boundary Γ_{out} and the physical wall of the vessel Γ_{wall}. Γ_{in} and Γ_{out} can possibly consist of more parts (like in a vascular bifurcation). Variables of interest are the velocity $\mathbf{u}$ and the pressure $P = \rho_f p$ which are assumed to obey the incompressible Navier-Stokes equations in Ω. Here we have denoted by ρ_f the fluid density. At this stage, we consider the steady problem. We assume to have velocity measures (Data) $\mathbf{u}^m$ available at N_s sites[1] $\mathbf{x}_i \in \Omega$. Following the general description given in the Introduction, we assume that the CV is represented by the inflow normal stress $\mathbf{h}$. This is an arbitrary choice, an extensive comparison with other choices is still to be done. Post-processing $f(\cdot)$ in this case is given by the Dirac delta distributions, such that $f(\mathbf{u})$ is the vector of the values of the computed velocity at the measurement sites. Then, the distance $dist(f(\mathbf{u}), \mathbf{u}^m)$ is defined as $\sum_{i=1}^{N_s} (\mathbf{u}(\mathbf{x}_i) - \mathbf{u}^m(\mathbf{x}_i))^2$. The control problem reads: Find

$$
\begin{aligned}
&\min_{\mathbf{h}} \mathscr{J}(\mathbf{u}, \mathbf{h}) = dist(f(\mathbf{u}), \mathbf{u}^m) + \text{Regularization}(\mathbf{h}) \\
&\text{s.t.} \quad \begin{cases} -\nabla \cdot (\nu \nabla \mathbf{u}) + (\mathbf{u} \cdot \nabla)\mathbf{u} + \nabla p = \mathbf{s} & \text{in } \Omega, \\ \nabla \cdot \mathbf{u} = 0 & \text{in } \Omega, \\ \mathbf{u} = \mathbf{0} & \text{on } \Gamma_{wall}, \\ -\nu \nabla \mathbf{u} \cdot \mathbf{n} + p\mathbf{n} = \mathbf{h} & \text{on } \Gamma_{in}, \\ -\nu \nabla \mathbf{u} \cdot \mathbf{n} + p\mathbf{n} = \mathbf{g} & \text{on } \Gamma_{out}, \end{cases}
\end{aligned}
\tag{2}
$$

where $\mathbf{n}$ denotes the outward unit vector normal to the boundary. A Newtonian rheology is supposed to hold, since it is a common assumption in large and medium vessels [23] and ν is the kinematic viscosity. Since we are considering fixed geometries, we assume homogeneous Dirichlet boundary conditions on Γ_{wall}. When solving problems in the form (2) there are in general two possibilities. In the first one, we first write the necessary conditions associated with the continuous constrained optimization problem, the so called *Karush Kuhn Tucker* (KKT) system [57, 34]. These are obtained by augmenting the original functional with the (variational formulation of) the constraint given by FW (in this case the steady Navier-Stokes problem), weighted by unknown multipliers and then by setting to zero the derivatives of the augmented functional with respect to the multipliers (so to obtain the *state problem*), to the variables (*adjoint problem*) and to CV (*optimality conditions*). Successively, the resulting problem is discretized (*Optimize then Discretize* - OD - approach). In the second approach, we first discretize the different components of the problem (the functional to be minimized and the constraints) and then perform the optimization

[1] Notice that we use the word "sites" for the location of measurements, as opposed to the word "nodes" for points where velocities are computed. We do not assume at this level particular positions for the sites, even though in the applications it is reasonable to assume that they are located on planes transverse to the blood stream.

of the discrete system (*Discretize then Optimize* - DO - approach). In [14] we compared the two strategies, and found that the DO is more efficient for the problem at hand. For this reason we proceed with the latter approach.

2.1.1 The discrete DA Oseen problem

Let us consider preliminarily the linear Oseen problem. The nonlinear convection term $(\mathbf{u}\cdot\nabla)\mathbf{u}$ is replaced with $(\beta\cdot\nabla)\mathbf{u}$, where β is a known advection field. The discretized optimization problem reads

$$\begin{aligned}&\min_{\mathbf{H}} \mathscr{J}(\mathbf{V},\mathbf{H}) = \frac{1}{2}\|\mathrm{D}\mathbf{V}-\mathbf{U}^m\|_2^2+\frac{a}{2}\|\mathrm{L}\mathbf{H}\|_2^2 \quad \text{where } \mathbf{V}=\begin{bmatrix}\mathbf{U}\\ \mathbf{P}\end{bmatrix},\ \mathrm{S}=\begin{bmatrix}\mathrm{C}+\mathrm{A}^\beta & \mathrm{B}^{\mathrm{T}}\\ \mathrm{B} & \mathrm{O}\end{bmatrix}\\ &\text{s.t. } \mathrm{S}\mathbf{V}=\mathrm{R}_{in}^{\mathrm{T}}\mathrm{M}_{in}\mathbf{H}+\mathbf{F}.\end{aligned} \tag{3}$$

Here, **U** and **P** are the discretization of velocity and pressure. In particular, we resort to an inf-sup compatible finite element (FE) discretization (see e.g. [66], Chapters 7, 9). **H** is the discretization of the control variable **h**. In formulating the minimization problem, we need to introduce some special matrices. Q is the discrete operator corresponding to f in (2), i.e. the matrix such that $[\mathrm{Q}\mathbf{U}]_i$ is the numerical solution evaluated at the site $\mathbf{x}_i$ and corresponded by the data $[\mathbf{U}^m]_i$. Matrix D is defined as $\mathrm{D}=[\mathrm{Q}\quad \mathrm{O}]$. R_{in} is a *restriction matrix* which selects the degrees of freedom (DOF) of the velocity **U** on Γ_{in}; M_{in} is the mass matrix restricted to inlet boundary nodes; C, A^β and B are the discretization of the diffusion, advection and divergence operators respectively. For $a>0$, $\frac{a}{2}\|\mathrm{L}\mathbf{H}\|_2^2$ is a Tikhonov regularization term (see e.g. [36]). Matrix L is such that $\mathrm{L}^{\mathrm{T}}\mathrm{L}$ is positive definite. The Lagrange functional associated with the problem (3) is

$$\mathscr{L}(\mathbf{V},\mathbf{H},\Lambda)=\frac{1}{2}\|\mathrm{D}\mathbf{V}-\mathbf{U}^m\|_2^2+\frac{a}{2}\|\mathrm{L}\mathbf{H}\|_2^2+\Lambda^{\mathrm{T}}(\mathrm{S}\mathbf{V}-\mathrm{R}_{in}^{\mathrm{T}}\mathrm{M}_{in}\mathbf{H}-\mathbf{F}), \tag{4}$$

where $\Lambda\in\mathbb{R}^{N_u+N_p}$ is the discrete Lagrange multiplier. The associated KKT system reads

$$\begin{cases}\mathrm{D}^{\mathrm{T}}(\mathrm{D}\mathbf{V}-\mathbf{U}^m)+\mathrm{S}^{\mathrm{T}}\Lambda=\mathbf{0}\\ a\mathrm{L}^{\mathrm{T}}\mathrm{L}\mathbf{H}-\mathrm{M}_{in}^{\mathrm{T}}\mathrm{R}_{in}\Lambda=\mathbf{0}\\ \mathrm{S}\mathbf{V}-\mathrm{R}_{in}^{\mathrm{T}}\mathrm{M}_{in}\mathbf{H}-\mathbf{F}=\mathbf{0}.\end{cases} \tag{5}$$

In [13] we proved the following proposition.

Proposition 1. *Sufficient conditions for the well-posedness of the discrete optimization problem are:*

1. $a>0$;
2. *for* $a=0$, $Null(\mathrm{D})\cap Range(\mathrm{S}^{-1}\mathrm{R}_{in}^{\mathrm{T}}\mathrm{M}_{in})=\{\mathbf{0}\}$ $(\star)$.

This result basically states that, in absence of regularization, well-posedness is guaranteed if enough measurement sites are placed at the inflow boundary. This proposi-

tion stems from the analysis of the system obtained after the elimination of $\mathbf{V}$ and Λ from the system (5) (the so-called *reduced Hessian*). In Fig. 2 we report the singular values of the reduced Hessian when the sufficient condition $(\star)$ is fulfilled (left) and violated (right). In the latter case, it is evident that in general a violation of such condition may lead to a *discrete ill-posed problem* [36].

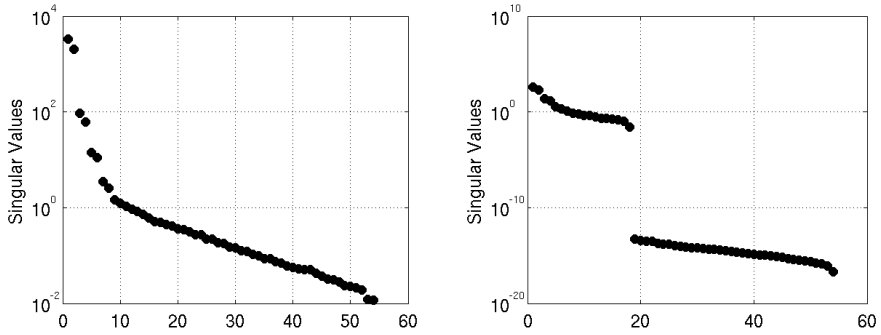

Fig. 2 Singular values of the reduced Hessian for a non regularized case ($a = 0$): on the left, the condition $(\star)$ is fulfilled, on the right it is violated.

On the contrary, no constraints need to be fulfilled when the Tikhonov regularization is active ($a > 0$). However, in practice, the selection of a requires to find the proper trade-off between the requirement to solve a well conditioned problem (large a) and to keep the perturbation of the original problem as small as possible (small a). A possible approach (see [8, 36]) is to select the parameter according to the discrepancy principle (DP), i.e. to select a in such a way that the perturbation of the regularization term affects the solution with the same order of the discrepancy induced by the noise. The proper choice of the parameter following this approach may be however computationally expensive. There is another possible way for forcing the well-posedness exploiting the result of Proposition 1. Actually, let us assume that some data are available at the inflow, not necessarily fulfilling the well-posedness sufficient condition $(\star)$. If we extend the given data to the entire set of DOF of Γ_{in} by interpolation of the available data (e.g. piecewise linear), the resulting problem satisfies condition $(\star)$. This results in fact in an additional term to the functional $\mathscr{J}$ that plays the role of a regularizing term (see [13]). A more extensive analysis of this approach, and the interplay between the interpolation and the noise affecting the original data is currently under investigation.

2.1.2 The nonlinear Navier Stokes problem

When we consider the nonlinear advection term $(\mathbf{u}\cdot\nabla)\mathbf{u}$ the problem becomes much more difficult since now we have a nonlinear constraint [57]. A possible approach is

to combine the DA procedure for the linear case with classical fixed point linearization schemes (i.e. Picard and Newton). Thus, the DA assimilation problem is solved iteratively. We report the simple case of the Picard method. Given a guess for the velocity at step k, say $\mathbf{U}_k$, we solve

$$\min_{\mathbf{H}_{k+1}} \frac{1}{2}\|\mathrm{D}\mathbf{V}_{k+1}(\mathbf{H}_{k+1}) - \mathbf{U}^m\|_2^2 + \frac{a}{2}\|\mathrm{L}\mathbf{H}_{k+1}\|_2^2 \quad \text{s.t.} \quad \mathrm{S}_k\mathbf{V}_{k+1} = \mathrm{R}_{in}^{\mathrm{T}}\mathrm{M}_{in}\mathbf{H}_{k+1} + \mathbf{F} \qquad \text{where } \mathrm{S} = \begin{bmatrix} \mathrm{C} + \mathrm{A}^{\mathbf{U}_k} & \mathrm{B}^{\mathrm{T}} \\ \mathrm{B} & O \end{bmatrix} \quad (6)$$

up to the fulfillment of a convergence criterion. When using the Newton method, the convergence strongly depends on the initial guess, so a common procedure is to perform a few Picard iterations (6) and use the resulting velocity as an initial guess for the Newton method. In our approach the loop for solving the nonlinear system is merged with the one for the optimization problem, thus reducing the computational cost. Numerical experience (next subsection) shows that convergence is not prevented by this further approximation. Other approaches can be however pursued, for an introduction to optimization with nonlinear constraints see [57].

2.2 Numerical results

We first present some simulations on an analytic test case, to investigate basic convergence properties of the DA procedure without and with the presence of the noise, in comparison with the FE convergence of the forward problem. Then we address a comparison between a classical Tikhonov regularization and the data interpolation method. Results have been obtained with the C++ finite element library `lifev` [16].

2.2.1 A consistency test

Let Ω be the domain $\Omega = [-0.5, 1.5] \times [0, 2]$ with a flow described by the analytical solution $\mathbf{u}_1(x,y) = 1 - e^{\lambda x}\cos(2\pi y)$, $\mathbf{u}_2(x,y) = \frac{\lambda}{2\pi}e^{\lambda x}\sin(2\pi y)$, $p(x,y) = \frac{1}{2}e^{2\lambda x} + C$, with $\lambda = \frac{1}{2}(\nu^{-1} - \sqrt{\nu^{-2} + 16\pi^2})$, and C is a constant chosen to give a zero mean pressure. Solution of the DA problem has been obtained by using inf-sup compatible FEs ($\mathbb{P}^1$bubble-$\mathbb{P}^1$). Regularization is obtained with L corresponding to the discrete gradient operator and a selected according to the DP. The nonlinear term has been solved by combining Picard and Newton methods.

As expected, in the noise-free case the assimilated velocity recovers the solution of the forward problem. In particular Fig. 3 shows that expected quadratic convergence rate for the L^2 norm of the velocity error when the mesh size Δx tends to 0. In case of noisy data (Gaussian white noise), the error dynamics changes. In particular, the error decreases as more data are available (see Fig. 4, left). We observe

that the convergence rate with respect to the number of sites N_s is of the order of $1/\sqrt{N_s}$. Moreover, when the number of sites and the mesh are fixed and we repeat the DA with different noise realizations, we observe a progressive convergence of the sample mean of the assimilated solution to the noise free solution, with a rate proportional to $1/\sqrt{N_r}$, being N_r the number or realizations. (see Fig. 4, right). Note that these results are consistent with the central limit theorem. More details can be found in [13].

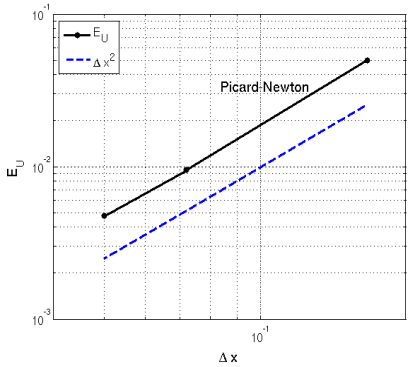

Fig. 3 Test of consistency for the DA procedure of velocity data: noise-free data. The accuracy of the computation is the same as for the solution of the FW problem.

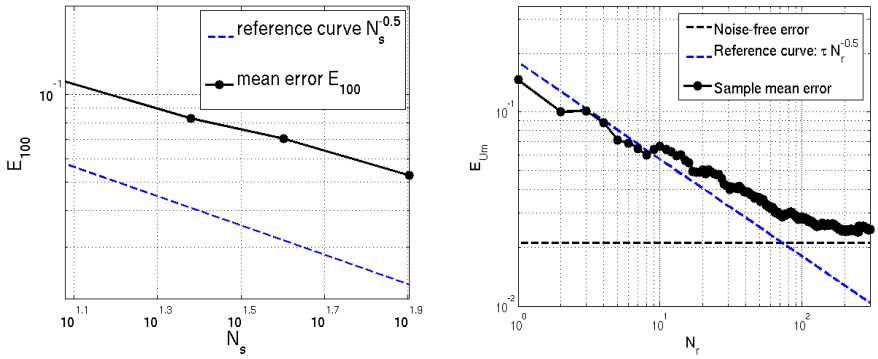

Fig. 4 Test of consistency for the DA procedure of velocity data: accuracy of the DA improves when the number of sites N_s (left) or of the noise realization N_r (right) increases.

2.2.2 Regularization & Interpolation

We compare the results obtained with the regularized problem (parameter a tuned again with the DP) and the interpolation of inflow data when these do not fulfill condition $(\star)$ of Proposition 1. In Table 1 (left) in correspondence of different choices of locations and number N_{in} of sites on Γ_{in}, we report the relative error and the number of iterations (`it`) for solving the reduced Hessian. The case where neither Tikhonov regularization or interpolation are performed is reported as a reference test. The addition of interpolated data on the DOF on Γ_{in} has the effect of forcing the well posedness of the problem, as can be inferred from the singular values of the reduced Hessian in the case reported in Figure 2. Also, results reported in Table 1 show that, in terms of accuracy, the interpolation procedure is comparable with Tikhonov regularization. This fact, combined with the computational saving associated with the generation of the interpolating function, as opposed to applying the DP, makes interpolation an efficient regularization technique, competitive with common available methods.

N_{in}	interpolation	a	E_U	`it`
14	no	0	0.068	14
14	no	0.021	0.061	15
14	yes	0	0.059	18
14	yes	0.021	0.056	16
8	no	0	0.199	11
8	no	0.038	0.137	18
8	yes	0	0.139	17
8	yes	0.038	0.129	17

SNR	$E_{\text{WSS,DA}}$	$E_{\text{WSS,FW}}$
100	0.2536	0.2667
20	0.2591	0.3030
10	0.2738	0.3861
5	0.3149	0.6114

Table 1 Left: Comparison of the results of a regularized DA vs a non-regularized interpolated DA. Right: **Relative** errors of the WSS computed with the DA procedure and a forward Navier-Stokes noisy simulation in a 2D carotid bifurcation for different values of the SNR.

2.2.3 Assimilated derived quantities in nontrivial geometries

In view of real hemodynamics applications, we present a demonstrative test case in non-trivial geometries (representing a 2D simplified model of the aortic arch and an arterial bifurcation). Since in these cases we do not have an analytical solution, we have computed a "reference" solution on an extremely fine mesh grid (using parabolic inflow conditions and homogeneous Neumann conditions at the outflow) in both cases. Successively, a noise with several values of Signal-to-Noise Ratio (SNR) has been added to the solution. This generates a set of noisy data to be assimilated represented by the black vector field in Figure 5, left. Results of the assimilation are significantly close to the reference solution. As a matter of fact, we consider as an index of the accuracy for the solution the ratio $E^*_{\mathbf{U}} = \frac{\|\mathbf{U}-\mathbf{U}_{ref}\|_2}{\|\mathbf{U}_{ref}\|_2}$. To

test the competitiveness of the DA procedure we compare the relative error of the assimilated velocity with the one of the velocity obtained from a forward simulation where noisy data on Γ_{in} are prescribed as a Dirichlet condition; in this case we obtain $E^*_{\mathbf{U}} = 8.1\text{e-}2$ and $E^*_{\mathbf{U}_{forward}} = 16.0\text{e-}2$. This pinpoints the role of DA as a process for de-noising the available data thanks to mathematical models. The DA procedure in fact corrects the measurements according to the physical principles underlying the mathematical model. This is evident not only for the primitive variable, but also checking non-primitive interesting quantities. In Figure 5, right, we report the vorticity map recovered from an assimilated velocity field on a geometry approximating an arterial bifurcation. For the same simulation, we check the accuracy of the WSS. Accuracy results are reported in Table 1, right. The WSS is retrieved in two ways. In the first case, we perform the DA procedure and use the assimilated velocity field for extracting the WSS. In the second case, we use again the inflow noisy data as boundary conditions for a forward computation of the incompressible Navier-Stokes equations on the same mesh where DA is performed. In particular, in the table we report the relative errors, i.e. the difference of the WSS compared with the noise-free reference solution on the fine mesh. It is evident that the DA leads to a more accurate estimate of the WSS, the improvement being more evident as the SNR gets smaller.

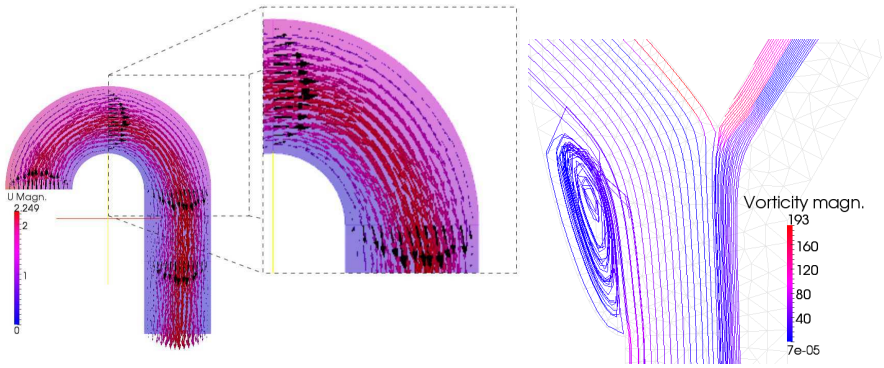

Fig. 5 Left: DA assimilation on 2D a curved domain. Black arrows are the data to be assimilated. The red arrows (colores refer to the pressure) are the results after the DA procedure. The results of DA are closer to the reference solution, highlighting the role of DA as a filtering procedure for the noise of the data. Right: vorticity in a 2D bifurcation computed by the DA procedure

2.3 Perspectives

Assimilation of (velocity) data into the simulation of an incompressible fluid is a problem whose interest goes beyond the specific medical applications, and different

methods are viable. In [37] Least Squares Finite Elements are used because of their versatility in managing different boundary conditions. In [26], merging of velocity data is carried out by using a "virtual" forcing term as CV. Here, we resorted to a control approach that in preliminary test cases provides promising results. Sufficient conditions for the well posedness of the linearized Oseen problem are given. Many challenges are however open by these preliminary results. Beyond (and before) an extensive use of DA in clinical practice, there are at least two main concerns that deserve an accurate consideration.

1. *Analysis of the impact of the noise.* An extensive analysis of this aspect is in order to identify the reliability of the results. Modeling the impact of uncertainty on the solution of partial differential equations is an up-to-date topic (see e.g. [55, 59] and the recent work [18], comparing Galerkin vs collocation methods). Different approaches can be pursued and different sources of noise should be considered, depending on the measurement devices (see e.g. [6] and Chapter 3 of [42]). A *sensitivity analysis* of quantities of interest such as the WSS on the noise affecting the data would clarify the robustness of the procedure to the perturbations. More advanced approaches are based on the moment method, the Bayesan approach, the polynomial chaos (see e.g. [79]). Extensive investigations on this aspects, with different approaches, will be carried out as a follow up of the present results.
2. *Unsteady problems.* When solving unsteady problems, following again a DO approach, we first discretize in time and at each instants solve the optimization problem. In this case, the extension of the method devised for the steady case is pretty immediate. However, possible computational concerns arise from the nesting of the time and the optimization loops. Selection of appropriate effective preconditioners is in order. Another issue refers to the initial conditions that in general are not known. In meteorological applications, these are included in the set of CV and used for driving the assimilation procedure. In cardiovascular applications an alternative approach consists of forcing periodicity of the solution. This approach will be investigated elsewhere.

3 Image Assimilation in a Moving Domain Simulation

Rigid-wall models for blood motion in arteries are often accurate enough for a quantitative analysis of hemodynamics (see e.g. [71]). However, there are situations in which the magnitude of the mechanical forces involved and the deformation experienced from the vessels cannot be neglected and their effects should be appropriately considered while modeling the coupled system.

The standard strategy to simulate the blood flow in a compliant vessel is to write the models for both the blood (the incompressible Navier-Stokes equations) and the wall (see e.g. [39]) together with appropriate matching conditions at the interface between the two domains (Fluid-Structure Interaction - FSI). At the numerical level, the coupled model is then solved either with a monolithic approach or by seg-

regated solvers managing iteratively the sequence of fluid and solid problems (see e.g. [28]). This strategy allows the accurate computation of both fluid and solid mechanics and is challenging from both the modeling and the numerical point of view. In fact, the constitutive laws for modeling the arterial wall still deserve extensive investigations especially in the presence of vascular pathologies (see e.g. [82]), not to mention the difficulty to obtain *in vivo* measurements that can accurately estimate the model parameters for an individual patient (see Sect. 4). Moreover, vessels are subject to external loads due to the presence of the surrounding tissues, which are in general unknown or not easy to model. We mention for example the effects of cardiac motion on the aortic arch. From the numerical point of view, the strongly heterogeneous nature of the problem raises issues concerning numerical stability and efficiency of FSI algorithms (see e.g. [10, 27]).

Here we consider an alternative approach based on a DA procedure, that exploits the technological development experienced in the last decade by medical imaging techniques. The advent of high resolution imaging devices allows the fast acquisition of 4D (space + time) images. From those images it is possible to reconstruct anatomical structures not just in one specific instant, but in multiple ones over the cardiac cycle. Following this approach, the vessel motion, instead of being computed, is retrieved from images and plugged into the Navier-Stokes solver. The main advantage of this approach is the direct inclusion into the simulations of patient-specific data, i.e. the motion of the vessel (depending on its mechanical characteristics and those of the surrounding organs). This is done through the use of medical images at a limited additional computational cost with respect to the case in which the geometry is assumed to be fixed. We will denote this approach 4D Image Based (4DIB). A similar technique has been proposed in [71, 76] where the authors apply this image-based motion approach to intra-cranial aneurysms and coronary arteries respectively, even if implementing different strategies for some steps of the procedure.

3.1 Mathematical and numerical formulation

The workflow of the 4DIB approach consists in the following steps (for more details, we refer to [64]). We assume to have an image set that represents the vessel of interest at several time frames $\{t_k\}$ within a heart beat.

1) *Segmentation* - Depending on the nature of the source images, their dimensionality and the complexity of the geometry to be reconstructed, segmentation can be performed on single 2D planes or directly on 3D datasets. Different segmentation methodologies and different ways to represent the final models are available. For an introduction, see [2, 6]. In the applications presented here, a level set technique was used for the 3D segmentation of vessels, specifically the segmentation tool available within the Vascular Modeling Toolkit (VMTK) software package [1]. At the end of this step, a triangulated surface is available for each time frame.

2) *Motion tracking* - This consists in solving a *registration problem* (see e.g. [22]), i.e. finding the alignment of the geometries of two consecutive time frames, so to have a displacement field that maps the points on the surface of the lumen at a given time frame to the surface in the subsequent one. This is another example of inverse problems that can be cast in the form of the feedback loop in the Introduction. For this reason, we detail this step in the next subsection.

3) *Simulation* - From the sequence of maps describing the motion of the surface points from one time frame to the subsequent one, the velocity of the boundary of the moving domain is estimated at the image acquisition times. Then, this is interpolated to define the velocity of the boundary at each time instant in the simulation. To ensure the continuity of the time derivative of the points velocity, a cubic spline time interpolation is chosen. The displacement and the grid velocity $\mathbf{w}$ of the whole domain, computed at each time step of the simulation, are obtained by the harmonic extension of the boundary fields. Once the domain motion is available, the incompressible Navier-Stokes equations for a Newtonian fluid in a moving domain can be written in the *Arbitrary Lagrangian Eulerian* (ALE) formulation (see, e.g., [40])

$$\begin{aligned} &\frac{\partial \mathbf{u}}{\partial t} - \nu \Delta \mathbf{u} + (\mathbf{u} - \mathbf{w}) \cdot \nabla \mathbf{u} + \nabla p = \mathbf{s}, && \text{in} \quad \Omega(t) \\ &\nabla \cdot \mathbf{u} = 0 && \text{in} \quad \Omega(t), \\ &\mathbf{u} = \mathbf{w} && \text{on} \quad \Gamma_w(t), \\ &+\text{Boundary Conditions} && \text{on} \quad \Gamma_{in}(t) \text{ and } \Gamma_{out}(t). \end{aligned} \tag{7}$$

On the wall the fluid velocity is prescribed equal to the vessel velocity (Dirichlet condition), while inflow and outflow boundary data can be retrieved by measures or designed to reproduce a physiological or pathological behavior.

3.1.1 Assimilation of segmented vascular surfaces

Registration is a procedure for aligning images taken from different devices, from different viewpoints or at different time instants. Many different methodologies exist depending on the source of images, their dimensionality and the type of movement to be recovered, particularly whether we have small or large deformations. In particular, a wide number of different approaches have been detailed for surface registration (see e.g. [49, 86, 9, 3]).

Here we resort to an algorithm relying upon a minimization procedure [22]. The registration is performed over 3D surfaces representing the vessel at the different time frames. More precisely, given M+1 time frames corresponding to M+1 triangulated surfaces, the tracking process consists in M registration steps between each couple of consecutive time steps. Within each stage the points of one surface, the *source surface* $\mathscr{S}$, are mapped to the subsequent one, called the *target surface* $\mathscr{T}$. A displacement field for the whole surface mesh is computed so that at the end of this tracking procedure, M displacement fields are available describing the vessel wall motion at the instants of the image acquisitions.

The map between two consecutive frames is computed by minimizing a functional in the form (1). In particular, let us denote with $\varphi(\cdot)$ the (unknown) map from $\mathscr{S}$ to $\mathscr{T}$. Referring to the feedback loop in the Introduction, the forward problem FW is the actual application of φ to the source surface $\mathscr{S}$ (Input), so that[2] $\mathbf{v} = f(\mathbf{v}) = \varphi(\mathscr{S})$. The Data are represented by the target surface $\mathscr{T}$. The control variable set CV is given by the mathematical representation of the map $\varphi(\cdot)$. This can be parametrically described by assuming, e.g., that it belongs to a functional finite dimensional space spanned by a basis function set ψ_i so that $\varphi = \sum a_i \psi_i$, being a_i real coefficients. In this case a_i are the CV. However, since the map is supposed to be strongly space-dependent, in [64] we resorted to a *non-parametric map* implicitly defined with a collocation approach by the position of the nodes on the source image. This means that the coordinates of the vertexes computed by the minimization process implicitly define the map point-wise. The map is then extended to the entire source surface by a piecewise linear interpolation of the values of the vertexes.

Finally, to complete the picture, we need to specify the definition of the distance between $\varphi(\mathscr{S})$ and the data $\mathscr{T}$ and the regularizing term. Different choices are available, strictly problem dependent. Let us introduce the distance of the image of a point on $\mathscr{S}$ to the surface $\mathscr{T}$ as

$$\delta(\varphi(\mathbf{x}), \mathscr{T}) = \inf\{\|\varphi(\mathbf{x}) - \mathbf{y}\| : \mathbf{y} \in \mathscr{T}\}, \quad \mathbf{x} \in \mathscr{S}. \tag{8}$$

The distance between $\mathscr{S}$ and $\mathscr{T}$ can be then defined as

$$dist(\varphi(\mathscr{S}), \mathscr{T}) \equiv \left(\frac{1}{|\mathscr{S}|} \int_{\mathscr{S}} (\delta(\varphi(\mathbf{x}), \mathscr{T}))^2 \, d\mathscr{S}(\mathbf{x}) \right)^{1/2} \tag{9}$$

where $|\mathscr{S}| := \int_{\mathscr{S}} d\mathscr{S}$ is a normalization factor. In practice the integral needs to be numerically approximated. For triangulated surfaces like $\mathscr{S}$ and $\mathscr{T}$ a reasonable and viable approximation is

$$dist(\varphi(\mathscr{S}), \mathscr{T}) = \sqrt{\frac{1}{n_S} \sum_j \min_i (d_{ji})^2} \tag{10}$$

where

$$d_{ji} = \mathrm{dist}(\varphi(\mathbf{x}_j), \mathrm{tri}_i)$$

is the distance from vertex j of $\mathscr{S}$ to triangle i in $\mathscr{T}$, n_S (n_T) is the number of vertexes (triangles) of $\mathscr{S}$ ($\mathscr{T}$). By using a tree search algorithm, it is possible the reduce the computational complexity to $\mathscr{O}(n_S \log(n_T))$ (see [4]).

This non-parametric registration by itself is in general ill-posed and multiple solutions are expected. Some of them are clearly unphysical and need to be filtered out. For this reason a regularizing term is introduced, forcing the solutions to be "physically acceptable" by adding some regularizing properties (see e.g. [63, 77]). In particular, we resort to a regularizing term stemming from a simplified physical

[2] the post-processing in this case is trivially the identity application.

model of the vascular wall as an elastic thin membrane [54] accounting for traction and bending internal forces. The membrane energy provides the regularizing term. In this way, displacements $\varphi(\cdot)$ that would cause a large increase to the membrane energy are heavily penalized (see [64]).

Additional constraints are required for preventing "flips" of triangles. Let

$$A_i = \text{area}(\text{tri}(\mathbf{x}, \mathbf{y}, \mathbf{z}))$$

be the area of the i^{th} triangle before deformation and x,y,z its corresponding vertexes. Correspondingly, let

$$\varphi(A_i) = \text{area}(\text{tri}(\varphi(\mathbf{x}), \varphi(\mathbf{y}), \varphi(\mathbf{z})))$$

be the area of the deformed i^{th} triangle.

Therefore, we add to the minimization of $\mathscr{J}$ the constraint of positive deformed area

$$C_i(\varphi) = \varphi(A_i) > 0. \tag{11}$$

The minimization problem has been solved by means of the L-BFGS procedure (Limited memory BFGS - see [57]), that requires only the computations of gradients and features (at least) a linear convergence even for non-smooth problems.

3.2 Numerical Results

In the following application a 4D computed tomography (CT) dataset of a human aorta was employed as image source. The dataset was acquired at Ospedale Maggiore in Milan (Italy) using a Siemens SOMATOM Definition Flash Dual-Source CT scanner, which was able to capture 10 time frames per cardiac cycle. The 4D image refers to a 72-year-old man with a diagnosed abdominal aneurysm and covers the entire length of the ascending, thoracic and abdominal aorta. From this dataset the portion of the aorta including the aortic arch and the thoracic aorta was considered for a simulation in a moving domain. The aorta was then segmented with VMTK at all the 10 time frames available, and the tracking procedure was applied to extract the 10 displacement fields describing the vessel wall motion over the cardiac cycle. Figure 6 represents some of the reconstructed surfaces at different time frames: they are simply superimposed prior to the registration procedure in order to highlight the misalignment due to their movement. Figure 7 depicts the results of the registration procedure (performed with an *ad hoc* Matlab code) for two consecutive surfaces. In the rightmost panel frame 1 has been mapped to frame 2.

Quantification of the errors of the registration process is reported in [64]. A more detailed analysis of the error as a function of the number of nodes n_S and triangles n_T used in each couple of frames is however missing and will be carried out elsewhere.

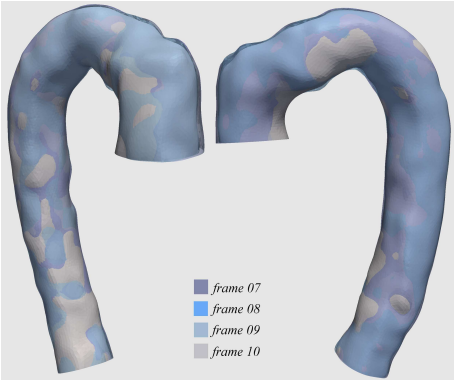

Fig. 6 Synopsis of the last 4 frames superimposed before tracking has been performed

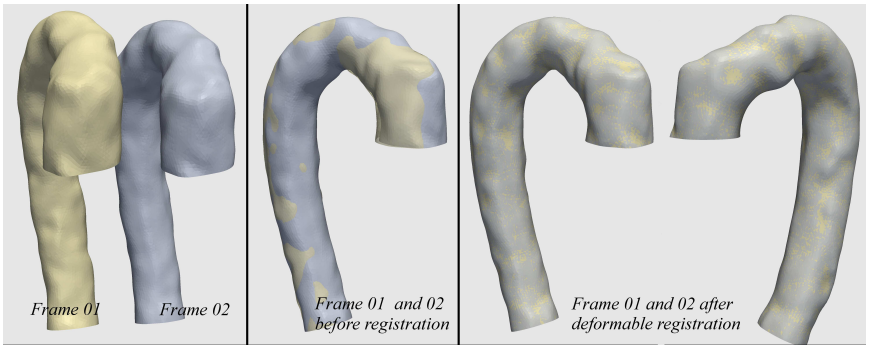

Fig. 7 Detail of two frames of the aorta before and after the registration

Numerical tests have been run with `LifeV` to evaluate the difference between the velocity and wall shear stress (WSS) fields computed with the 4DIB approach and those computed on a rigid domain simulation. The choice of aorta is motivated by the fact that here the vessel deformation is relevant (mostly as a consequence of the motion of the heart) and is supposed to affect significantly the blood motion. To discretize the ALE Navier-Stokes system, we have chosen a first-order time advancing scheme and a finite element approximation for the space dependence ($\mathbb{P}^1$ for the pressure and $\mathbb{P}^1$bubble for the fluid velocity).

Both the velocity and the WSS fields exhibited a considerable difference with respect to the rigid domain case, as shown in Figure 8. In particular, the relative L^2 norm of the difference between the 4DIB fields and the rigid domain fields has an average over the cardiac cycle of 84.52% for the velocity and 83.18% for the WSS.

We also performed an *in-silico* consistency test of the 4DIB approach with respect to a FSI simulation, assumed to be the reference benchmark solution. In particular we have first run a FSI simulation, obtaining the fluid velocity and pressure fields and the displacement of the vessel wall. Then, we have used this displacement as if it was retrieved from images to feed a 4DIB simulation, with the same

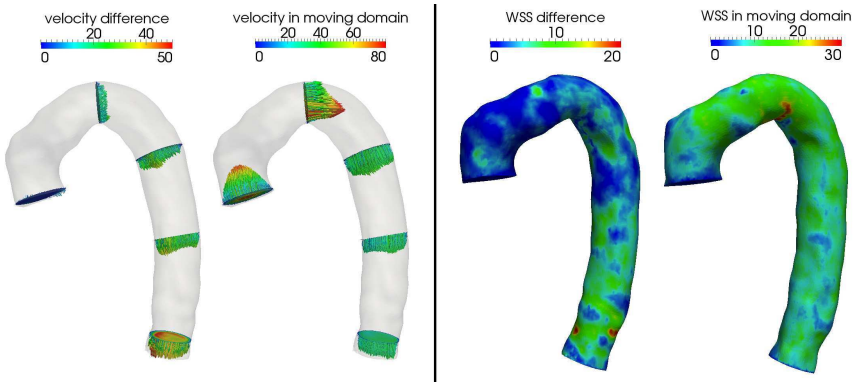

Fig. 8 Left panel: difference (in cm/s) between the fluid velocity computed in the rigid domain simulation and the one computed in the 4DIB simulation (left); velocity (in cm/s) computed with the 4DIB approach (right); both at peak systole. Right panel: difference (in dyne/cm^2) between the WSS computed in the rigid domain simulation and the one computed in the 4DIB simulation (left); WSS (in dyne/cm^2) computed with the 4DIB approach (right); both at peak systole.

inflow/outflow boundary conditions and fluid properties as in the FSI case. The comparison of the results obtained with the two approaches has shown a good agreement, being below 1% of relative difference, on both velocity and WSS. Notice that the computational time required by the 4DIB simulation is significantly smaller than the one required by the FSI simulation (see [64]).

These tests show that (i) when a relevant motion affects the vessel like in the aortic case, the 4DIB approach is a viable way for a more realistic description of the blood flow than a rigid simulation provided that available data can be properly assimilated; (ii) the results of the 4DIB method are consistent with the results of a traditional FSI simulation when the displacement field of the structure is the same.

3.2.1 A practical workaround for reduced data sets

The 4DIB approach presented here is based on the availability of 4D image data sets as it is made possible by recent devices. One of the limitations of the approach is that as for now only a few instruments are actually able to produce this kind of data set. This aspect will be naturally overcome in the future with a larger diffusion of those devices. However, a natural question arises now: is it possible to pursue a similar approach even for reduced data sets? The following example presents a possible workaround currently used in the analysis of the relations between WSS and atherogenesis, in collaboration with the group of Dr. W.R. Taylor at the Emory School of Medicine (Atlanta, GA, USA). In this case a mouse aorta was acquired with magnetic resonance imaging (MRI). The whole 3D geometry of the aorta and its main branches was reconstructed at a single time step, while the motion in time of the aorta was retrieved only at a number of locations along its centerline. At these

points, in fact, the cross sections of the aorta were acquired in time by means of cine MRI sequences (Figure 9). The lumen in the corresponding 2D slices was segmented and its area computed for each acquisition instant. The time evolution in time of each cross section area was then reconstructed by fitting these data with a cubic spline interpolation. The displacement of the whole aorta was suitably interpolated from the data available at each slice. More precisely, under the assumption that the longitudinal and circumferential motion of the vessel is negligible, and that each aortic section is circular, the time pattern of the area provided data on the wall displacement in correspondence of each slice. The displacement over the entire vessel at each instant was eventually retrieved by a cubic spline interpolation along the axial coordinate.

Since no information was available on the motion of the branching vessels, their presence was included in the simulation with the definition of proper stress boundary conditions for the fluid equations.

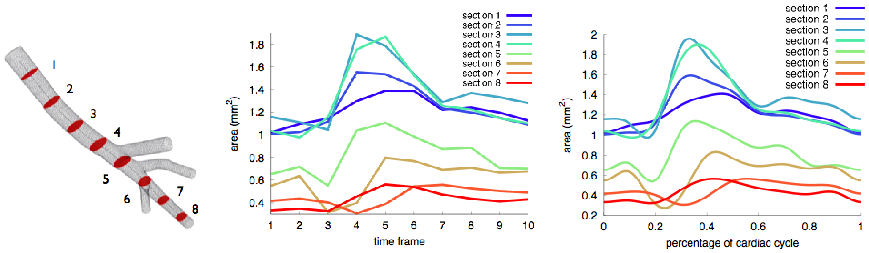

Fig. 9 Left: an example of a vascular structure of interest, the abdominal aorta in a mouse. In correspondence to the highlighted cross-sections, measurements of the arterial wall movement are available in the form of MRI cine sequences. Center: for each highlighted cross-section, the values of the area in time are plotted. The cross sectional area has been computed from MRI cine sequences, after segmentation of the images at each acquisition time. Right: The time pattern of the cross-section area has been reconstructed by fitting the values obtained from the images.

Again, we compared the results obtained from a simulation of blood flow in a mouse aorta under the assumption that the vessel geometry is fixed, with the results of a simulation in moving domain with the "reduced" 4DIB approach.

The results of the rigid wall simulation (Figure 10, left) showed that areas of disturbed flow characterize the branching points of the proximal abdominal aorta. High values of the *oscillatory shear index* (OSI - see e.g. [43]) were computed in very localized regions at the ostia of the main aortic branches. The hemodynamic environment was characterized overall by relatively low shear load. The results of the moving domain simulation (Figure 10, right) provided an insight into the effects of the vessel dilatation in the region of interest. As a measure of the dilatation, the difference between the maximum and minimum radius (over the cardiac cycle) of each section was computed, and normalized by the minimum radius. The average value of this indicator on the eight slices was 35%, being maximum in the proximal abdominal aorta (even more than 40%). When taking into account the movement of

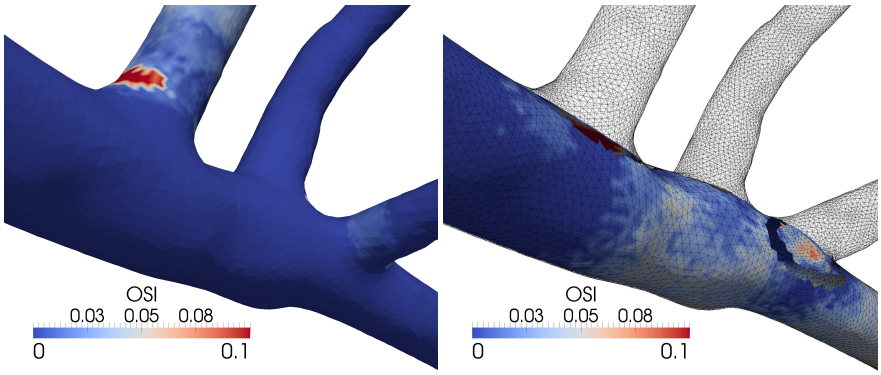

Fig. 10 Oscillatory Shear Index (OSI, [43]) on the arterial wall of the proximal abdominal aorta. Left: Results of the rigid wall simulation. Right: Results of the moving wall simulation.

the vessel, the computed WSS showed a similar spatial pattern but overall a smaller magnitude compared to the rigid wall case. The ostia of the main aortic branches were not included in the moving domain simulation due to the lack of information on their movement. However, the computed WSS was significantly more oscillating with respect to the rigid wall simulation in the entire proximal abdominal aorta, and in particular in the region surrounding the branching points. This was indeed experimentally found to be a typical site for atherosclerosis development.

Despite being only in a preliminary stage, these results suggest that neglecting the movement of the arterial wall may have a significant impact on the estimation of clinically relevant features, such as the presence of oscillatory flow. Validation of these results is ongoing.

3.3 Perspectives

The 4DIB approach has some important drawbacks and limitations. It requires a large data set of images, which is not always available, even if some problem-specific workarounds can be devised to overcome this problem, as presented in Section 3.2.1. Moreover, this approach does not provide information on solid mechanics of the walls and it is therefore suitable when the focus of the study is on the flow features alone. However, this DA methodology splits the pipeline into a phase dedicated to the “offline” retrieval of the motion from images and a phase for the computation of the dynamics of the fluid alone, which has important computational advantages with respect to full FSI simulations. Furthermore, this approach could guarantee a reasonable reliability to patient-specific simulations of blood flow when the vascular motion is determined by external components that could not readily be included in a wall model, or more in general, when individual mechanical parameters for a single patient are not available.

Many open problems deserve to be addressed. As we have mentioned, a complete analysis of the accuracy of the registration process and how the registration errors affect the computation of fluid dynamics still needs to be carried out. In this context, it is particularly relevant the correlation of the numerical procedure with the noise affecting the image acquisition and segmentation. Using the terminology in [74] this DA procedure can be considered as a *frame-to-frame pseudo-observational approach*. More mathematically advanced methods advocated in [74] which entail an integrated variational assimilation of data and images similar to the ones introduced in Sect. 2 could be considered as a future development.

4 Variational Parameter Estimation

Since mathematical and numerical models are earning more relevance in medical applications and are used as patient-specific tools, a precise estimation of individual physical parameters featured by the equations is needed. Moreover, by themselves, some parameters can play the role of landmarks of pathologies. This is for instance the case of the stiffness of soft tissues in detecting breast cancer. Significant changes of the stiffness of the tissue can identify the presence of tumors. On the other hand, a small value of the compliance of the tissue could be an indicator of atherosclerosis or hypertension, while an increase of the stiffness of the left ventricle wall is a clear marker of *diastolic dysfunction*, which can lead to an increase of the end diastolic left ventricle pressure and, possibly, to heart failure (see e.g. [29, 75]). This has motivated sophisticated image-based diagnostic approaches, such as the *elastography* (see e.g. [50, 5, 58, 32]).

Either for a direct diagnostic purpose or for an individual-based evaluation to be used in numerical simulations, a precise estimation of biological parameters *in vivo* is still a challenging problem demanding appropriate mathematical tools. In this section we suggest a DA procedure. The starting point is that the parameters of interest are complicated functions of measurable quantities. For instance, the compliance of a tissue affects in a non trivial way its displacement, the latter being retrievable from images. In some cases (as in elastography) we can prescribe the forces inducing a measured displacement and formulate an inverse problem in the form: given the force and the consequent displacement, find the stiffness (or more precisely the Young modulus, in the case of a linear elastic material) that fits at best the experimental stress-strain data. In other cases, practical reasons prevent the knowledge of some of the ingredients of this inverse problem. For instance, the natural periodic motion of a vessel is the result of the interaction with the blood (and the other tissues), in turn forced by the heart action. The forces exerted on the vascular wall by the blood are not explicitly known but can be included in a mathematical model of the FSI, as a function of (available) velocity/pressure values on the boundary of the region of interest. The basic idea of DA approach is then to use numerical simulations for bridging available data to the ingredients needed for solving the inverse parameter-estimation problem.

In the case of the vascular stiffness, usable data are the images of the vessel displacement (as in Sect. 3) and velocity and pressure (Sect. 2) on the boundary. Numerical simulations allow to compute the forces on the wall and eventually to solve an inverse problem. We present here a first step in this direction. However, it is worth stressing that this DA approach has potentially a more general use than for the evaluation of the vascular compliance (that can be currently achieved in several ways), for different (and more numerous) sets of parameters.

4.1 Mathematical and numerical formulation

We formulate the problem of estimating the compliance of a linearly elastic membrane filled by an incompressible fluid as follows. Let Ω be the volume of interest of the fluid, where we assume the incompressible Navier-Stokes equations (7) to hold. The membrane Γ_w is a portion of $\partial\Omega$, i.e. a 2D surface for a 3D fluid, which is assumed to obey the equation for an elastic membrane

$$\rho_w \frac{\partial^2 \eta}{\partial t^2} + E\theta\eta = s_w, \tag{12}$$

where η is the membrane displacement assumed to be normal to Γ_w, ρ_w is the density of the solid, s_w is the stress exerted by the fluid and by surrounding tissues (the latter will be neglected in the following), and θ is a function of the mean and Gaussian curvatures of the membrane and accounts for the transversal membrane effects (see [56]). Young modulus E is the parameter we want to estimate. The fluid subproblem (7) and the membrane one (12) are coupled at the FS interface Γ_w by the continuity of the normal stress and of the velocity

$$-\nu\left(\nabla\mathbf{u} + \nabla\mathbf{u}^T\right)\cdot\mathbf{n} + p = s_w, \qquad \frac{\partial\eta}{\partial t}\mathbf{n} = \mathbf{u} \quad \text{on } \Gamma_w. \tag{13}$$

The grid velocity $\mathbf{w}$ is the computed as the harmonic extension of $\dfrac{\partial\eta}{\partial t}\mathbf{n}$ in Ω.

Now, we assume that the displacement of the vessel can be measured by a set of time resolved images and the sequence of steps *segmentation + registration*, as we have done in the previous section. After an appropriate cubic spline interpolation (see Sect. 3), we have the time dependent displacement field $\eta^m(t,\mathbf{x})$ defined on Γ_w, that represents the Data. Displacement η^m is assimilated with the numerical model as indicated by the feedback loop in the Introduction. The FW problem is given by the system of equations (7,12,13), the unknown being $\mathbf{v} = [\mathbf{v}, p, \eta]$. The post processing function selects the displacement, i.e. $f(\mathbf{v}) = \eta$. The CV is represented by the Young modulus E. The functional $\mathscr{J}$ reads

$$\mathscr{J} = \int_0^T \int_{\Gamma_w} (\eta - \eta^m)^2 \, d\mathbf{x}\, dt + \text{Regularization},$$

where T is the heart beat duration. Again, the regularizing term enhances the mathematical and numerical properties of the problem. A possible form is

$$\alpha \int_0^T \int_{\Gamma_w} \left(E - E_{ref}\right)^2 d\mathbf{x}\, dt,$$

where α is the usual parameter weighting the effect of the regularizing term on the minimization process and E_{ref} is a reference value of the Young modulus available for instance from the literature. If we assume *a priori* that the CV is positive, we can also consider the term

$$\alpha \max_{\mathbf{x}\in\Gamma_w, t>0} \left(\log\left(\frac{E}{E_{ref}}\right)\right)^2.$$

In both cases the regularizing term penalizes the distance between the control variable E and the reference value for the Young modulus E_{ref}.

The solution of this minimization problem is not trivial in many respects. Hereafter we present a first possible approach, under some simplifying assumptions. Even though in the more general case, the Young modulus can be function of time and space, in the sequel we assume

1. E constant in time in the interval $[0,T]$, significant changes of the compliance in an artery being expected over a longer time scale;
2. E piecewise constant in space, as we distinguish basically healthy and pathological tissues featuring different values of compliance, each value being reasonably constant in each subregion.

Computational and algorithmic aspects of the numerical solution of the minimization problem are challenging. Here we resort to the workflow *Time Discretize, then Optimize, then Space Discretize*. This means that we first discretize in time the problem by collocating the minimization process at selected time instants t^k. Then we perform the minimization, by computing the KKT system for the space-continuous problem. Finally, we discretize the KKT system. In this way, the variational procedure for the minimization does not involve adjoint backward-in-time problems (see [34]) and the differentiation of the Lagrangian functional does not require to perform differentiation of the domain Ω (shape derivatives), since at each instant the domain Ω is frozen. The anticipated drawback of this approach is that the effect of noise over the time interval is not damped by a least square minimization, being the problem collocated pointwise at t^k. Post-processing for the estimates of E obtained at each step is required for filtering out the error. An extensive analysis of different solution methods for this problem is however an important follow up in this context.

After time discretization, at each instant t^k the problem reads (hereafter we omit to specify the time index k for the sake of readability): Find the piecewise constant function E defined on Γ_w that minimizes the functional

$$\mathscr{J} = \int_{\Gamma_w} (\eta - \eta^m)^2 \, d\mathbf{x} + \alpha \max_{\mathbf{x}\in\Gamma_w} \left(\log\left(\frac{E}{E_{ref}}\right)\right)^2$$

$$\text{s.t.} \quad \begin{cases} \gamma_1 \mathbf{u} + (\mathbf{u}-\mathbf{w})\nabla\cdot\mathbf{u} - \nu\nabla\cdot\left(\nabla\mathbf{u}+\nabla\mathbf{u}^T\right) + \nabla p = \mathbf{g}_1 & \text{in } \Omega, \\ \nabla\cdot\mathbf{u} = 0 & \text{in } \Omega, \\ (\gamma_2 + \gamma_3 E\theta)\,\mathbf{u}\cdot\mathbf{n} - p + \nu(\nabla\mathbf{u}+\nabla\mathbf{u}^T)\mathbf{n} = g_2, \quad \mathbf{n}\times\mathbf{u}\times\mathbf{n} = 0 & \text{on } \Gamma_w, \\ +\text{Boundary Conditions} & \text{on } \Gamma_{in} \text{ and } \Gamma_{out}. \end{cases} \tag{14}$$

The functions $\mathbf{g}_1$, g_2 and γ_i depend on the time discretization. In the previous system, the FSI problem has been simplified by eliminating the displacement, leading to a fluid problem with Robin boundary conditions, as proposed in [56].

The explicit computation of the KKT system for this problem and its generalization to the case of a 3D thick elastic structure are reported in [60]. We have analyzed different choices for the space of the admissible CV (E). In particular, for the piecewise constant and piecewise linear cases, we can prove the following Proposition.

Proposition 2. *For $\alpha > 0$ the KKT system associated with the minimization problem has at least one solution.*

After the space discretization, the KKT system yields a non-linear algebraic minimization problem. In particular we can use again the gradient-based BFGS method (see e.g. [57]). For more details, see [60].

4.2 Numerical results

We present two test cases on simplified geometries, solved again with the library LifeV. These test cases have the role of assessing the overall performances of the method on synthetic data, in view of a more extensive analysis using real medical images. The "synthetically measured" displacement field η_{fwd} is therefore generated by a preliminary numerical simulations with a prescribed Young modulus. Successively, the data are perturbed in order to mimic noise featuring different SNR.

In the first set of simulations (already reported in [60]), we solve the problem in a cylinder of radius $R = 0.5\ cm$ and height $H = 6\ cm$. The computation is performed in 2D under the assumption of axial symmetry of the problem. We impose the pressure drop $\Delta p = 10^4\, dyne/cm^2$ for the first 5 ms between the inlet and the outlet of the vessel. We set $\rho_f = 1\, g/cm^2$, $\rho_w = 1.1\, g/cm^2$, $\mu = 0.035\, Poise$, $h = 0.02\, cm$ and $\Delta t = 0.001\, s$.

Figure 11 shows the geometry and the pressure along a longitudinal section of the cylinder, for different time instants.

The optimization problem has been solved by using the BFGS algorithm over 10 time steps, corresponding to the first 10 ms of the simulation. We run the optimization problem for 10 realizations of the noise. In Table 2, we report the average over

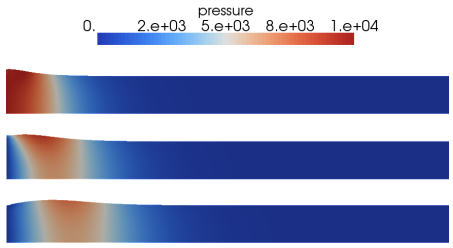

Fig. 11 2D axisymmetric case, Forward simulation. Geometry at time $t = 4$ *ms*, $t = 6$ *ms* and $t = 8$ *ms*. Colored with blood pressure.

the 10 realizations of the estimated values of E and the relative error. Different initial guesses E_0 and different SNR are considered. These results show that for large values of the SNR, the estimate obtained by the method is accurate. Moreover, the BFGS applied to the membrane case is pretty robust with respect to the noise, both in terms of accuracy and convergence.

Other 2D cases on non-trivial geometries (like a bifurcation) have been reported in [60].

$\downarrow E_0 \setminus SNR \rightarrow$	10	5	3	2.5
$10^7\, dyne/cm^2$	1.302 ± 0.027	1.314 ± 0.054	1.330 ± 0.085	1.357 ± 0.103
	0.2%	1.1%	2.3%	4.4%
$10^5\, dyne/cm^2$	1.303 ± 0.027	1.315 ± 0.056	1.330 ± 0.087	1.348 ± 0.115
	0.2%	1.1%	2.3%	3.7%

Table 2 Standard deviation of the ten estimates (to be multiplied by 10^6, top) and mean percentage error (bottom) for different values of the initial guess E_0 for the Young modulus and of the percentage P. Exact E is $1.3 \cdot 10^6\, dyne/cm^2$.

We now consider the three dimensional geometry shown in Figure 12, representing a simplified aorta. This geometry consists of a cylinder of radius $1.5cm$ and height $10cm$ and half a torus with curvature radius $4cm$. The pressure field and the geometry displacement are shown in Figure 12. As before, we estimate the compliance using the displacement of the forward simulation perturbed by an artificial noise. In Table 3 we report the results. In the 3D case, the methods seems to be

$\downarrow E_0 \setminus SNR \rightarrow$	20	10	5
$10^7\, dyne/cm^2$	1.32 ± 0.05	1.35 ± 0.12	1.24 ± 0.7
	1.5%	3.8%	9.5%

Table 3 Mean and standard deviation of five estimates (to be multiplied by 10^6, top) and mean relative error for different values of the Young modulus and of SNR. Exact E is $1.3 \cdot 10^6\, dyne/cm^2$.

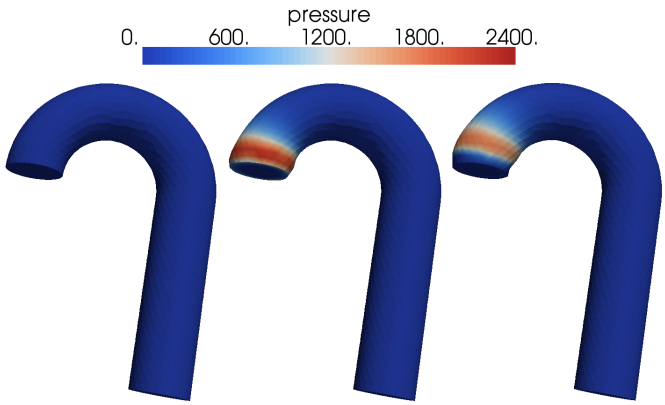

Fig. 12 3D simplified aorta, Forward simulation. Geometry at time $t = 0$ *ms*, $t = 16$ *ms* and $t = 22$ *ms*. Colored with blood pressure.

more sensitive to the noise. However even with a noise with SNR=5, the parameter estimation is accurate enough for most of clinical applications.

4.3 Perspectives

As the preliminary results indicate, the assimilation of data and numerical models is a worthwhile approach for estimating patient-specific parameters to be used either for detecting possible anomalies or performing individual-based numerical simulations. Here, numerical differential models play the role of a bridge between the measurable data and the unknown parameters. There are many critical issues at the computational level to be addressed. Even if practical applications in general demand for less accuracy than the one usually considered acceptable from the numerical viewpoint, the impact of the noise is supposed to play a relevant role on the reliability of the entire approach. Moreover, the frequency of sampling of images, currently driven by technological limits, has probably a major impact on the accuracy of the results.

From the computational viewpoint, in these preliminary applications we resorted to standard numerical tools like the BFGS method. Extension of this approach to real 3D cases rises new issues on the computational effectiveness of the methods. An extensive comparison among different possible options (in particular for the sequence of optimization and discretization steps) and different possible algorithms is required for a massive use of these methods in practice.

A long term follow up of the present research is the extension of this optimization procedure to more complex sets of CV, such as the configuration and geometrical features of the cardiac fibers. In fact, we mention here that one of the open challenging problems in heart imaging and modeling is the estimation of the orientation of

the fibers driving the mechanical contraction and the electrical potential propagation in the cardiac tissue.

5 Conclusion

A mathematically sound adoption of numerical models for investigating the vascular blood dynamics originates from pioneering works in the late 80s (among the others, see e.g. [61, 62, 67]). At that time, numerical simulations were carried out in idealized domains, moving from basic geometrical primitives to realistic shapes of regions of interest. Simulations were intended to provide an insight to physiological and pathological dynamics for a better understanding of the most relevant diseases. The impact of these simulations was mostly at a qualitative level, since data and geometries were realistic but not patient-specific. Successively, in the '90s, the advent of new imaging technologies and corresponding numerical methods allowed the introduction of "patient-specific" simulations. The geometry of the single patient at a given instant was reconstructed from digital subtraction angiographies or computed tomographies and used as the computational domain, possibly together with individual measures of data for the boundary conditions. This "sequential" merging of data and simulations (i.e., *first* the data, *then* the simulations fed by the data) led to a more quantitative relevance of numerical models, closer to the clinical activity. Reliability of numerical models have been progressively increased by removing many of the simplifying assumptions postulated in the first simulations, e.g. rigid geometries or Newtonian rheology (see e.g. [23]).

The development of more sophisticated mathematical and numerical models has been corresponded by the development of more sophisticated measurements and imaging tools. Nowadays, these instruments provide more data and more images, so that it is reasonable to think to a further step, moving from a "sequential" to an "integrated" use of data and simulations. The DA approach entails measures and images to be used not just for providing initial and boundary conditions, but to drive the results by a sophisticated integration with the mathematical models. The outcome of this process is an assimilated result where not only numerical computation is strictly consistent with the individual data, but the noise affecting the data has been filtered out by the mathematical modeling.

The "integrated" paradigm, which is well developed in other contexts such as the weather forecasting, opens many challenging problems at the methodological and practical level. The quality of the data in terms of their size, location in space and frequency in time plays obviously a major role in the mathematical properties (well posedness) of the assimilation problem (see [48]). Moreover, the noise that invariably affects the data has an impact on the reliability of the entire process. A precise evaluation of this aspect is strictly related to both the type of data and the methods used for the assimilation procedure. This leads to analyze and solve partial differential equations with stochastic terms (see e.g. [83, 84, 85, 18]).

When the assimilation problem is solved with variational methods, the mathematical strcuture almost invariably can be represented as a feedback control loop. The effective numerical solution of inverse problems in this form presents many open concerns to be properly addressed (see [57]).

In this chapter we have presented three basic examples sharing this control-loop structure, motivated by ongoing collaborations with medical doctors. The first preliminary results enlighten the great potential of DA as a way for improving both the reliability of numerical results and the quality of measures. As we have pointed out, a certified reliability is crucial since bioengineering and medical communities are increasingly resorting to scientific computing for taking decisions (see [20]). The accomplishment of the new integrated paradigm - requiring new advanced and increasingly interdisciplinary research - represents an exciting challenge of cardiovascular mathematics for the years to come.

Acknowledgements Marina Piccinelli and Alessandro Veneziani thank Emory University Research Committee for the support of the Project "Image based numerical fluid structure interactions simulations in computational hemodynamics". The research of C. Vergara has been (partially) supported by the ERC Advanced Grant N.227058 MATHCARD. The authors wish to thank Marijn Brummer (Emory Childrean Healthcare of Atlanta), Eldad Haber (University of British Columbia, Canada), Robert Taylor (Emory School of Medicine), Michelle Consolini (Emory School of Medicine), Michele Benzi (Emory University), Max Gunzburger (Florida State University), George E. Karniadakis (Brown University).

References

1. L. Antiga et al. Vascular modeling toolkit, website. www.vmtk.org.
2. L. Antiga, D. A. Steinman, and J. Peiró. From image data to computational domain. In *Cardiovascular Mathematics*, MM&S, chapter 4. Springer, Italy, 2009. L. Formaggia, A. Quarteroni, A. Veneziani (eds.).
3. M.A. Audette, F.P. Ferrie, and T.M. Peters. An algorithmic overview of surface registration techniques for medical imaging. *Medical Image Analysis*, 4(3):201–217, 2000.
4. C. Barber, D. Dobkin, and H. Hudhanpaa. The quickhull program for convex hulls. *ACM Transactions on Mathematical Software*, 22:469–483, 1996.
5. Paul E Barbone and Assad A Oberai. Elastic modulus imaging: some exact solutions of the compressible elastography inverse problem. *Physics in Medicine and Biology*, 52(6):1577, 2007.
6. M. Bertero and M. Piana. Inverse problems in biomedical imaging: modeling and methods of solution. In *Complex Systems in Biomedicine*, chapter 1, pages 1–33. Springer, 2006. A. Quarteroni, L. Formaggia, A. Veneziani (eds.).
7. J. Blum, F.X. Le Dimet, and I.M. Navon. *Data Assimilation for Geophysical Fluids*, volume XIV of *Handbook of Numerical Analysis*, chapter 9. Elsevier, 2005.
8. T. Bonesky. Morozov's discrepancy principle and Tikhonov-type functionals. *Inverse Problems*, 25:015015, 2009.
9. L.G. Brown. A survey of image registration techniques. *ACM computing surveys (CSUR)*, 24(4):325–376, 1992.
10. P. Causin, J.F. Gerbeau, and F. Nobile. Added-mass effect in the design of partitioned algorithms for fluid-structure problems. *Computer Methods in Applied Mechanics and Engineering*, 194(42-44):4506–4527, 2005.

11. D. Chapelle and P. Moireau. Robust filter for joint state parameters estimation in distributed mechanical system. *Discrete and Continous Dynamical Systems*, 23(1-2):65–84, 2009.
12. Frederica Darema. Dynamic data driven applications systems (dddas) - a transformative paradigm. In *ICCS (3)*, page 5, 2008.
13. M. D'Elia, M. Perego, and A. Veneziani. A variational data assimilation procedure for the incompressible Navier-Stokes equations in hemodynamics. Technical Report TR-2010-19, Department of Mathematics & CS, Emory University, 2010.
14. Marta D'Elia and A. Veneziani. Methods for assimilating blood velocity measures in hemodynamics simulations: Preliminary results. *Procedia Computer Science*, 1(1):1231–1239, 2010. ICCS 2010.
15. P.M. den Reijer, D. Sallee, P. van der Velden, E. Zaaijer, W.J. Parks, S. Ramamurthy, T. Robbie, G. Donati C., Lamphier, R. Beekman, and M. Brummer. Hemodynamic predictors of aortic dilatation in bicuspid aortic valve by velocity-encoded cardiovascular magnetic resonance. *Journal of Cardiovascular Magnetic Resonance*, 12(1):4, 2010.
16. S. DeParis et al. Lifev - library for finite elements, website. www.lifev.org.
17. R.P. Dwight. Bayesian inference for data assimilation using Least-Squares Finite Element methods. In *IOP Conference Series: Materials Science and Engineering*, volume 10, page 012224. IOP Publishing, 2010.
18. H.C. Elman, C.W. Miller, E.T. Phipps, and R.S. Tuminaro. Assessment Of Collocation And Galerkin Approaches To Linear Diffusion Equations With Random Data. *International Journal for Uncertainty Quantification*, 1(1), 2011.
19. H.W. Engl, M. Hanke, and A. Neubauer. *Regularization of inverse problems*. Springer Netherlands, 1996.
20. Ahmet Erdemir, Trent Guess, Jason Halloran, Srinivas C. Tadepalli, and Tina M. Morrison. Recommendations for reporting finite element analysis studies in biomechanics. http://www.imagwiki.nibib.nih.gov/mediawiki/index.php?title=Reporting_in_FEA, 2010.
21. Vincent J. Ervin and Hyesuk Lee. Numerical approximation of a quasi-Newtonian Stokes flow problem with defective boundary conditions. *SIAM J. Numer. Anal.*, 45(5):2120–2140, 2007.
22. B. Fischer and J. Modersitzki. Ill-posed medicine: an introduction to image registration. *Inverse Problems*, 24:034008, 2008.
23. L. Formaggia, A. Quarteroni, and A. Veneziani, editors. *Cardiovascular Mathematics*, volume 1 of *MM&S*. Springer, Italy, 2009.
24. L. Formaggia, A. Veneziani, and C. Vergara. A new approach to numerical solution of defective boundary value problems in incompressible fluid dynamics. *SIAM Journal on Numerical Analysis*, 46(6):2769–2794, 2008.
25. L. Formaggia, A. Veneziani, and C. Vergara. Flow rate boundary problems for an incompressible fluid in deformable domains: formulations and solution methods. *Computer Methods in Applied Mechanics and Engineering*, 199(9-12):677–688, 2010.
26. K. Funamoto, Y. Suzuki, T. Hayase, T. Kosugi, and H. Isoda H. Numerical validation of mr-measurement-integrated simulation of blood flow in a cerebral aneurysm. *Ann Biomed Eng*, 37(6):1105–1116, 2009.
27. L. Gerardo-Giorda, F. Nobile, and C. Vergara. Analysis and optimization of robin-robin partitioned procedures in fluid-structure interaction problems. *SIAM J Num Anal*, 48(6):2091–2116, 2010.
28. J.F. Gerbeau and M. Fernandez. Algorithms for fluid-structure interaction problems. In *Cardiovascular Mathematics*, MM&S, chapter 9. Springer, Italy, 2009. L. Formaggia, A. Quarteroni, A. Veneziani (eds.).
29. E.R. Giuliani, B.J. Gersh, M.D. McGoon, D.L. Hayes, and H.V. Schaff. *Mayor Clinic Practice of Cardiolgy*. Mosby Publisher, St.Luis, 1996.
30. R. Glowinski, C.H. Li, and J.L. Lions. A numerical approach to the exact boundary controllability of the wave equation (I) Dirichlet controls: Description of the numerical methods. *Japan Journal of Industrial and Applied Mathematics*, 7(1):1–76, 1990.
31. R. Glowinski and J.L. Lions. Exact and approximate controllability for distributed parameter systems. *Acta numerica*, 3:269–378, 1994.

32. Nachiket H Gokhale, Paul E Barbone, and Assad A Oberai. Solution of the nonlinear elasticity imaging inverse problem: the compressible case. *Inverse Problems*, 24(4):045010, 2008.
33. L. Grinberg, Anor T., Cheever E., Marsden. J.P., and G E Karniadakis. Simulation of the human intracranial arterial tree. *Phil. Trans. R. Soc. A*, 367:2371–2386, 2009.
34. M.D. Gunzburger. *Perspectives in flow control and optimization*. Society for Industrial Mathematics, 2003.
35. M. Gurvitz, R.K. Chang, S. Drant, and V. Allada. Frequency of aortic root dilation in children with a bicuspid aortic valve. *The American journal of cardiology*, 94(10):1337–1340, 2004.
36. P.C. Hansen. *Rank-deficient and discrete ill-posed problems: numerical aspects of linear inversion*. Society for Industrial Mathematics, 1998.
37. JJ Heys, TA Manteuffel, SF McCormick, M. Milano, J. Westerdale, and M. Belohlavek. Weighted least-squares finite elements based on particle imaging velocimetry data. *Journal of Computational Physics*, 229(1):107–118, 2010.
38. J.I.E. Hoffman and S. Kaplan. The incidence of congenital heart disease. *Journal of the American College of Cardiology*, 39(12):1890, 2002.
39. G.A. Holzapfel, T.C. Gasser, and R.W. Ogden. A new constitutive framework for arterial wall mechanics and a comparative study of material models. *Journal of elasticity*, 61(1):1–48, 2000.
40. T. J. R. Hughes, W. K. Liu, and T. K. Zimmermann. Lagrangian-Eulerian finite element formulation for incompressible viscous flows. *Computer Methods in Applied Mechanics and Engineering*, 29(3):329–349, 1981.
41. K. Ide, P. Courtier, M. Ghil, and A.C. Lorenc. Unified notation for data assimilation: Operational, sequential and variational. *Journal of Meteorological Society of Japan*, 75(Special):181–189, 1997.
42. J. Kaipio and E. Somersalo. *Statistical and Computational Inverse Problems*. Springer, 2005.
43. DN Ku, DP Giddens, CK Zarins, and S Glagov. Pulsatile flow and atherosclerosis in the human carotid bifurcation. positive correlation between plaque location and low oscillating shear stress. *Arterioscler Thromb Vasc Biol*, 5(3):293–302, 1985.
44. J.L. Lions. *Optimal control of systems governed by partial differential equations*. Springer Verlag, 1971.
45. J.L. Lions. Are there connections between turbulence and controllability? In *9th INRIA International Conference, Antibes*, 1990.
46. J.L. Lions. Exact Controllability for distributed systems. Some trends and some problems. *Applied and Industrial Mathematics: Venice-1, 1989*, page 59, 1991.
47. J.L. Lions. Remarks on approximate controllability. *Journal d'Analyse Mathématique*, 59(1):103–116, 1992.
48. J.L. Lions. On the controllability of distributed systems. *Proc Natl Acad Science*, 94:4828–4835, 1997.
49. JB Maintz and M.A. Viergever. A survey of medical image registration. *Medical image analysis*, 2(1):1–36, 1998.
50. A. Manduca, R. Muthupillai, P. J. Rossman, and J. F. Greenleaf. Visualization of tissue elasticity by magnetic resonance elastography. *Lecture Notes in Computer Science*, 1131:63, 1996.
51. P. Moireau and D. Chapelle. Reduced-order Unscented Kalman Filtering with application to parameter identification in large-dimensional systems. *ESAIM: Control, Optimisation and Calculus of Variations*, 2010.
52. P. Moireau, D. Chapelle, and P. Le Tallec. Joint state and parameter estimation for distributed mechanical systems. *Computer Methods in Applied Mechanics and Engineering*, 197(6-8):659–677, 2008.
53. P. Moireau, D. Chapelle, and P. Le Tallec. Filtering for distributed mechanical systems using position measurements: perspectives in medical imaging. *Inverse Problems*, 25:035010, 2009.
54. W. Mollemans, F. Schutyser, J. Van Cleynenbreugel, and P. Suetens. Tetrahedral mass spring model for fast soft tissue deformation. *Surgery Simulation and Soft Tissue Modeling*, pages 1002–1003, 2003.

55. F. Nobile and R. Tempone. Analysis and implementation issues for the numerical approximation of parabolic equations with random coefficients. *International Journal for Numerical Methods in Engineering*, 80:979–1006, 2009.
56. F. Nobile and C. Vergara. An effective fluid-structure interaction formulation for vascular dynamics by generalized Robin conditions. *SIAM J Sc Comp*, 30(2):731–763, 2008.
57. Jorge Nocedal and Stephen Wright. *Numerical Optimization*. Springer, apr 2000.
58. Assad A Oberai, Nachiket H Gokhale, Sevan Goenezen, Paul E Barbone, Timothy J Hall, Amy M Sommer, and Jingfeng Jiang. Linear and nonlinear elasticity imaging of soft tissue in vivo : demonstration of feasibility. *Physics in Medicine and Biology*, 54(5):1191, 2009.
59. J. Tinsley Oden, Ivo Babuska, Fabio Nobile, Yusheng Feng, and Raul Tempone. Theory and methodology for estimation and control of errors due to modeling, approximation, and uncertainty. *Computer Methods in Applied Mechanics and Engineering*, 194(2-5):195–204, 2005. Selected papers from the 11th Conference on The Mathematics of Finite Elements and Applications.
60. M. Perego, A. Veneziani, and C. Vergara. A variational approach for estimating the compliance of the cardiovascular tissue: An inverse fluid-structure interaction problem. Technical Report TR-2010-18, Department of Mathematics & CS, Emory University, www.mathcs.emory.edu, 2010.
61. K. Perktold and D. Hilbert. Numerical simulation of pulsatile flow in a carotid bifurcation model. *Journal of Biomedical Engineering*, 8(3):193–199, 1986.
62. Karl Perktold. On numerical simulation of three-dimensional physiological flow problems. Technical report, Ber. Math.-Stat. Sekt. Forschungsges. Joanneum 280, 1-32 , 1987.
63. D. Perperidis, R.H. Mohiaddin, and D. Rueckert. Spatio-temporal free-form registration of cardiac MR image sequences. *Medical Image Analysis*, 9(5):441–456, 2005.
64. M. Piccinelli, L. Mirabella, T. Passerini, E. Haber, and A. Veneziani. 4d image-based cfd simulation of a compliant blood vessel. Technical Report TR-2010-27, Department of Mathematics & CS, Emory University, www.mathcs.emory.edu, 2010.
65. A. Quarteroni, L. Formaggia, and A. Veneziani, editors. *Complex Systems in Biomedicine*. Springer, Italy, 2006.
66. Alfio Quarteroni and Alberto Valli. *Numerical Approximation of Partial Differential Equations*. Springer, 1994.
67. CCM Rindt, F.N. Vosse, A.A. Steenhoven, JD Janssen, and RS Reneman. A numerical and experimental analysis of the flow field in a two-dimensional model of the human carotid artery bifurcation. *Journal of biomechanics*, 20(5):499–509, 1987.
68. F. Robicsek, M.J. Thubrikar, J.W. Cook, and B. Fowler. The congenitally bicuspid aortic valve: how does it function? Why does it fail? *The Annals of thoracic surgery*, 77(1):177–185, 2004.
69. Allan R. Robinson and Pierre F.J. Lermusiaux. Overview of data assimilation. Technical Report 62, Harvard University, Cambridge, Massachusetts, aug 2000.
70. M. Sermesant, P. Moireau, O. Camara, J. Sainte-Marie, R. Andriantsimiavona, R. Cimrman, DLG Hill, D. Chapelle, and R. Razavi. Cardiac function estimation from MRI using a heart model and data assimilation: advances and difficulties. *Functional Imaging and Modeling of the Heart*, pages 325–337, 2005.
71. D.M. Sforza, R. Lohner, C. Putman, and J.R. Cebral. Hemodynamic analysis of intracranial aneurysms with moving parent arteries: Basilar tip aneurysms. *International Journal for Numerical Methods in Biomedical Engineering*, 2010.
72. C. A. Taylor and M.T. Draney. Experimental and Computational Methods in Cardiovascular Fluid Mechanics. *Ann Rev Fluid Mech*, 36:197–231, 2004.
73. C.A. Taylor, M.T. Draney, J.P. Ku, D. Parker, B.N. Steele, K. Wang, and C.K. Zarins. Predictive medicine: Computational techniques in therapeutic decision-making. *Computer Aided Surgery*, 4(5):231–247, 1999.
74. O. Titaud, A. Vidard, I. Souopgui, and F.X. Le Dimet. Assimilation of image sequences in numerical models. *Tellus A*, 62(1):30–47, 2010.
75. E.J. Topol, editor. *Textbook of Cardiovascular Medicine*. Lippincott-Raven Publisher, Philadelphia-New York, 1998.

76. R. Torii, J. Keegan, N.B. Wood, A.W. Dowsey, A.D. Hughes, G.Z. Yang, D.N. Firmin, S.A.M.G. Thom, and X.Y. Xu. MR Image-Based Geometric and Hemodynamic Investigation of the Right Coronary Artery with Dynamic Vessel Motion. *Annals of biomedical engineering*, pages 1–15, 2010.
77. M. Vaillant and J. Glaunes. Surface matching via currents. In *Recent advances in parallel virtual machine and message passing interface: 11th European PVM/MPI Users' Group Meeting, Budapest, Hungary, September 19-22, 2004: proceedings*, page 381. Springer-Verlag New York Inc, 2004.
78. F. Viscardi, C. Vergara, L. Antiga, S. Merelli, A. Veneziani, G. Puppini, G. Faggian, A. Mazzucco, and G.B.Luciani. Comparative Finite Element Model Analysis of Ascending Aortic Flow in Bicuspid and Tricuspid Aortic Valve. *Artificial Organs*, 34(12):1114–1120, 2010.
79. R.W. Walters and L. Huyse. Uncertainty analysis for fluid mechanics with applications, 2002.
80. C. Ward. Clinical significance of the bicuspid aortic valve. *Heart*, 83(1):81, 2000.
81. G. Welch and G. Bishop. An introduction to the Kalman filter. *University of North Carolina at Chapel Hill, Chapel Hill, NC*, 1995.
82. R. Wulandana and AM Robertson. An inelastic multi-mechanism constitutive equation for cerebral arterial tissue. *Biomechanics and Modeling in Mechanobiology*, 4(4):235–248, 2005.
83. D. Xiu and G.E. Karniadakis. Modeling uncertainty in flow simulations via generalized polynomial chaos. *Journal of Computational Physics*, 187(1):137–167, 2003.
84. D. Xiu, D. Lucor, C.H. Su, and G.E. Karniadakis. Stochastic modeling of flow-structure interactions using generalized polynomial chaos. *Journal of Fluids Engineering*, 124:51, 2002.
85. Xiu D. and Karniadakis G.E. Modeling uncertainty in steady state diffusion problems via generalized polynomial chaos. *Computer Methods in Applied Mechanics and Engineering*, 191(43):4927–4948, 2002.
86. B. Zitova and J. Flusser. Image registration methods: a survey. *Image and vision computing*, 21(11):977–1000, 2003.
87. E. Zuazua. Controllability of partial differential equations and its semi-discrete approximations. *Dynamical Systems*, 8(2):469–513, 2002.